A multi-domain dynamical model for cone-shaped dielectric elastomer loudspeakers

Giacomo Moretti[a], Gianluca Rizzello[a], Marco Fontana[b], and Stefan Seelecke[a]

[a]Intelligent Material Systems Laboratory, Saarland University, Saarbrücken, Germany
[b]TeCIP Institute, Scuola Superiore Sant'Anna, Pisa, Italy

ABSTRACT

This paper presents a multi-physics model of an electrostatic loudspeaker system that combines the acoustic diaphragm and the actuator into a lightweight dielectric elastomer (DE) membrane. The focus is set on the so-called cone-shaped DE actuator (DEA) topology, which features a self-standing compact architecture, free from pneumatic loading systems, and is potentially suitable for integration onto complex surfaces and structures. We propose an axial-symmetrical lumped-parameter nonlinear model of the cone DEA structural dynamics, and use it to predict the acoustic pressure field generated by the speaker. We then present a case study in which the model is used to predict the linearised mode shapes of a reference DEA, evaluate their effect on the acoustic frequency response, and compare the harmonic distortions resulting from different driving strategies.

Keywords: dielectric elastomer, acoustics, loudspeaker, modelling, vibrations

1. INTRODUCTION

Dielectric elastomer (DE) actuators are soft variable-capacitance transducers that exploit Coulomb forces to produce controllable deformations in rubber-like dielectric membranes.[1] Thanks to their high energy density and lightweight, they are regarded as a promising actuator technology in different mechatronic applications, such as soft robots[2] or fluidic systems.[3]
A notable feature of DE actuators (DEAs) is their ability to work over a broad frequency range, from fractions of hertz potentially up to several thousand hertz.[1] Based on this, since the early stage of their technological history dielectric elastomers have been considered a promising technology for acoustic applications, such as unconventional loudspeakers.[4,5] In contrast with conventional speakers, DE loudspeakers can integrate the acoustic diaphragm and the actuator into a single soft structure, which relies on electrostatically-driven deformations. This opens up the possibility of developing flexible, compact and extremely lightweight acoustic drivers, suitable, among other, to be embedded into complex structures or textiles.

In the past, different concepts of DE loudspeaker have been proposed and tested. Most of these concepts rely on a circular DE membrane topology, on which a bubble-like initial deformation is impressed through a pressurisation/depressurisation.[4–9] Other layouts include flat-electrode,[10] buckling membrane,[11] and cone-shaped DEA speakers.[12]
In spite of these experimental proofs-of-concept, modelling and numerical analysis of DE speakers have been scarcely investigated. Recently, Garnell et al.[9,13] investigated for the first time the complex electro-elasto-acoustic interactions occurring in pneumatically-biased DE speakers. With the aim of weighting the effect of coupled elasto-acoustic interactions, they used a linear modelling approach, which proved very effective in predicting the DE loudspeaker frequency response, still without considering the effect of DEAs' nonlinear dynamics on the harmonic distortions.[1]

This paper presents a theoretical model of a conical DE diaphragm obtained through an out-of-plane deformation of a flat DE membrane. Although the cone-shaped DEA has been largely investigated for low-frequency actuator applications,[14,15] its high-frequency structural response and application on DE-based loudspeakers is limited to a few experimental observations.[12,16] Compared with inflated-membrane DE speakers, this topology

Send correspondence to G.M. E-mail: giacomo.moretti@imsl.uni-saarland.de

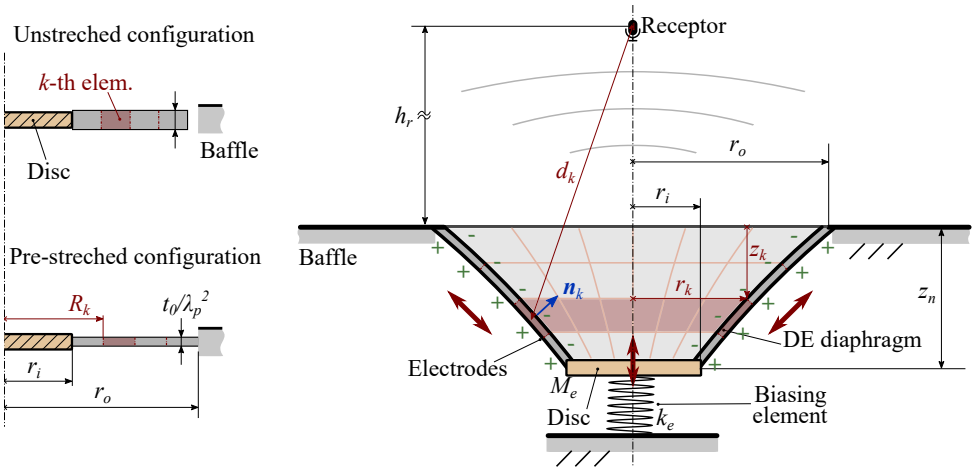

Figure 1: Layout of the cone-shaped DEA loudspeaker. The DEA is built by pre-stretching a flat annular membrane over two concentric frames (left), and creating an out-of-plane deformation by means of an elastic element (right). In the model formulation, the flat membrane is ideally divided into concentric elements. For the acoustic model, attention is focused on a receptor point located on the DEA axis.

does not use pressure regulation systems to provide the DE membrane with the required pre-load, and is potentially more suitable for integration onto complex structures.
A model of the DEA structural dynamics is formulated by discretising the DEA domain into sub-portions, and resorting to Lagrange equations to model their dynamics. The radiated sound pressure is rendered via the well-known Rayleigh theory.[17] Attention is restricted to axial-symmetrical deformations, which are expected to provide the most significant contribution to the radiated pressure.[13]
The presented formulation lends itself to analytical studies of the modal shape and frequency response of the system. Thanks to the lagrangian formulation, the model is able to capture the essential features of a DE loudspeaker dynamics even with a coarse discretisation of the domain, potentially requiring lower computational cost compared with off-the-shelf finite element codes. Compared with previously available models of the cone DEA,[15] our model is able to predict high-order complex mode shapes. Compared with available DEA speaker models,[13] this model accounts for the DEA nonlinear response, hence enabling the analysis of acoustic harmonic distortions.

The paper is structured as follows. Sect. 2 presents the layout of the cone-shaped DEA loudspeaker. Sect. 3 introduces a multi-degree-of-freedom lumped-parameter model for the DEA electro-elastic response and dynamics, and a model of the radiated acoustic pressure. Sect. 4 presents a case study on a reference device, including the analysis of the system acoustic frequency response and the evaluation of different driving strategies in terms of harmonic distortion. Sect. 5 draws the conclusions.

2. LAYOUT OF THE CONE-SHAPED DE LOUDSPEAKER

A cone-shaped DEA[14,15] consists in a planar annular DE membrane, coated by stretchable electrodes, with the outer perimeter attached on a fixed frame with radius r_o, and the inner perimeter connected to a rigid disc with radius r_i. The inner disc can move in the axial direction causing the DE membrane to assume a nearly conical shape (see Fig. 1). In the equilibrium configuration, the cone DEA is mechanically biased by an elastic element (e.g., a pre-tensioned spring), which brings the central disc at an equilibrium distance z_n from the membrane outer perimeter. In the flat configuration (i.e., with no elastic elements or external forces applied), the membrane holds a uniform biaxial pre-stretch λ_p. Indicating with t_0 the DE thickness in the undeformed state and assuming the DE material incompressible,[14] the thickness of the membrane in the flat configuration is t_0/λ_p^2.

Applying a voltage on the DEA electrodes, the the DE membrane further deforms out-of-plane, causing the distance of the central and the outer frames to increase. This “pumping” motion is exploited in any low-frequency

dynamic application of the cone-DEA. At highly dynamic regimes, in the presence broadband voltage excitation, other deformation patterns, involving variations in the membrane profile curvature,[18] may become relevant.

When a cone DEA is used as a loudspeaker, the membrane outer perimeter is attached on a planar baffle (e.g., the wall of a cabinet). For modelling simplicity, we hereby consider the case in which the speaker lies on an open infinite perfectly-reflecting baffle (Fig. 1(right)). The DE speaker can be mounted on a cabinet, but the analysis of this scenario would require a more sophisticated analysis of the pressure field within the cabinet, and is thus not conisdered in this work.

3. MULTI-DOMAIN MODEL OF A CONE-SHAPED DE DIAPHRAGM

This section presents a multi-physics model of the cone-shaped DEA loudspeaker. The model consists of two sub-blocks: 1) a multi-degree-of-freedom model of the cone-DEA dynamics, taking the driving voltage as the input and returning the velocity of a fixed number of nodes on the DEA surface; and 2) a simplified model of the radiated acoustic pressure, which uses the velocities of the DEA nodes as the input and predicts the radiated pressure.
Here, we do not account for the effect of the radiated sound pressure on the DE diaphragm dynamics, i.e., we neglect the effect of the acoustic impedance due to the fluid motion.[13] This contribution might be not negligible in DE loudspeakers made of thin lightweight membranes,[13] and will be thus included in the future.

The model is formulated in the time-domain, under the assumption of axial-symmetry, and it accounts for non-linearities due to the DEA electro-elastic response.

3.1 Electro-elastic model of the diaphragm dynamics

As opposed to lumped-parameter models of the cone DEA,[14,15] which use a single degree-of-freedom (DoF) approximation, we hereby formulate a multi-DoF model which relies on a discretisaton of the geometry.
We make the following assumptions: 1) The DE is an incompressible viscoelastic material, whose elastic response is modelled by an hyperelastic model;[14] the viscous response is rendered in a simplified way through a nonlinear Kelvin-Voigt rheological model.[19] 2) The DE diaphragm electrically behaves as an ideal parallel plate capacitor (with non-uniform thickness). The effect of electrodes resistivity and leakage currents is here neglected.

With reference to Fig. 1, we ideally divide the DE membrane into n concentric elements. We call R_k the inner radius of the $k-$th element in the flat pre-stretched configuration ($k=1$ indicates the outer element, whose external diameter is r_o, $k=n$ indicates the inner element, with internal diameter $r_n = r_i$). In a generic deformed configuration (Fig. 1 right), the inner edge of the $k-$th element lies at a distance r_k from axis and z_k from the equilibrium plane (z_n thus denotes the position of the central rigid disc).
The stretches on the $k-$th element in the meridian, circumferential and thickness direction respectively read as:

$$\lambda_{1k} = \lambda_p \frac{\sqrt{(r_k - r_{k-1})^2 + (z_k - z_{k-1})^2}}{R_{k-1} - R_k}, \quad \lambda_{2k} = \lambda_p \frac{r_k + r_{k-1}}{R_{k-1} - R_k}, \quad \lambda_{3k} = \frac{1}{\lambda_{1k}\lambda_{2k}}, \tag{1}$$

where the third equation owes to incompressibility.

We hereby consider the following the vector $\mathbf{q} \in \mathbb{R}^{2n-1}$ of generalised coordinates: $\mathbf{q} = [r_1, \dots, r_{n-1}, z_1, \dots, z_n]^\intercal$, and we define the lagrangian function $\mathcal{L}$ for the DEA system as follows:

$$\mathcal{L}(\dot{\mathbf{q}}, \mathbf{q}) = K(\dot{\mathbf{q}}) - U_m(\mathbf{q}) + \frac{V^2}{2} C(\mathbf{q}) \tag{2}$$

where K is the system kinetic energy; U_m is the elastic potential energy; and the third term is a generalised electrostatic potential energy contribution (or co-energy), equal to the energy supplied to the DEA by the power supply minus the electrostatic potential energy.[14] C in the third term is the DEA total capacitance which is a function of the current configuration $\mathbf{q}$. The voltage V on the DEA electrodes is a control variable (input), and is independent of the generalised coordinates. We assume that a uniform voltage V is applied on the whole electrode. The formulation could be however easily extended to the case of multi-channel DEAs with individually controlled electrode portions.

The kinetic energy is the sum of the kinetic energies of the single elements, K_k $(k = 1, \dots, n)$ plus the energy of the central disc:

$$K = \sum_k K_k + \frac{1}{2} M_e \dot{z}_n^2, \tag{3}$$

where M_e is the mass of the moving disc. For simplicity, we assume that each element is subject to a linear velocity distribution. Be $R \in [R_k, R_{k-1}]$ a generic point on the $k-$th element. The following expressions hold for the radial and axial velocity distributions $(v_{rk},\ v_{zk})$, and the kinetic energy K_k of the element:

$$\begin{gathered} v_{rk} = \frac{\dot{r}_{k-1} - \dot{r}_k}{R_{k-1} - R_k}(R_{k-1} - R) + \dot{r}_{k-1},\ v_{zk} = \frac{\dot{z}_{k-1} - \dot{z}_k}{R_{k-1} - R_k}(R_{k-1} - R) + \dot{z}_{k-1}, \\ K_k = \frac{1}{2}\rho_e \frac{t_0}{\lambda_p^2} \int_{R_k}^{R_{k-1}} \left(v_{rk}^2 + v_{zk}^2\right) 2\pi R \, \mathrm{d}R \end{gathered} \tag{4}$$

where ρ_e is the membrane equivalent DEA density (normalised on the dielectric thickness), generally different from the DE material density because of the contribution of the electrodes. An analytic expression for K_k (here omitted for conciseness) can be easily found by algebraic manipulation of (4), which depends solely on $\dot{r}_{k-1},\ \dot{r}_k,\ \dot{z}_{k-1},\ \dot{z}_k$. The elastic energy of the DEA reads as:

$$U_m = \sum_{k=1}^{n} \Omega_k \Psi(\lambda_{1k}, \lambda_{2k}) + \frac{1}{2} k_e \left(l_e - z_n\right)^2, \tag{5}$$

where $\Omega_k = \pi(R_{k-1}^2 - R_k^2)t_0/\lambda_p^2$ is the constant volume of the $k-$th element, Ψ is the DE material strain-energy function, k_e and l_e are parameters describing the biasing element (here, a linear spring). $\Psi = \Psi(\lambda_1, \lambda_2)$ is a function of the stretches, with a mathematical form given by a hyperelastic model. U_m is a function of the generalised coordinates $\mathbf{q}$ through the stretches (see Eq. (1)).
The DEA capacitance is the sum of the elements capacitance, $C = \sum_k C_k$, where:

$$C_k = \frac{\varepsilon S_k^2}{\Omega_k},\ \text{with } S_k = \pi(r_k + r_{k+1})\sqrt{(r_k - r_{k-1})^2 + (z_k - z_{k-1})^2} \tag{6}$$

where ε is the DE material permittivity and S_k is the area of an element's lateral surface.
Expressions (1), (4), (6) take a slightly different form in case $k = 1$ and $k = n$, which is here omitted for simplicity.

The equations of motion of the DEA system (namely, Lagrange's equations) read as:

$$\frac{\mathrm{d}}{\mathrm{d}t}\frac{\partial \mathcal{L}}{\partial \dot{\mathbf{q}}} - \frac{\partial \mathcal{L}}{\partial \mathbf{q}} = \mathbf{Q}_v \tag{7}$$

where t is time, and $\mathbf{Q}_v$ is a vector of dissipative loads owing to the DE material viscosity. We assume that the instantaneous dissipated power $\mathcal{P}_d$ due to the elastomer viscosity is a quadratic function of the stretch rates, namely:

$$\begin{gathered} \mathcal{P}_d = \eta \sum_{k=1}^{n} \Omega_k \left(\frac{(\dot{\lambda}_{1k})^2}{\lambda_{1k}} + \frac{(\dot{\lambda}_{2k})^2}{\lambda_{2k}} \right) = \dot{\boldsymbol{\lambda}}^\intercal \mathbf{D} \dot{\boldsymbol{\lambda}},\ \text{with} \\ \mathbf{D} = \eta\ \mathrm{diag}\left(\frac{\Omega_1}{\lambda_{11}}, \dots, \frac{\Omega_n}{\lambda_{1n}}, \frac{\Omega_1}{\lambda_{21}}, \dots, \frac{\Omega_n}{\lambda_{2n}} \right),\ \text{and } \boldsymbol{\lambda} = [\lambda_{11}, \dots, \lambda_{1n}, \lambda_{21}, \dots, \lambda_{2n}]^\intercal. \end{gathered} \tag{8}$$

where η is a viscous coefficient such that the viscous component of the Cauchy stress reads as $\sigma_{v,ik} = \eta\dot{\lambda}_{ik}$ for $i = 1, 2$. Eq. (8) is equivalent to a nonlinear Kelvin-Voigt model,[19] in which the material is modelled as a network of purely elastic and purely viscous elements connected in parallel. $\mathcal{P}_d$ can be expressed in terms of the generalised loads as $\mathcal{P}_d = -\dot{\mathbf{q}}^\intercal \mathbf{Q}_v$. Since the stretches only depend on $\mathbf{q}$ (see (1)): $\boldsymbol{\lambda} = \boldsymbol{\lambda}(\mathbf{q})$, the following expressions for $\mathbf{Q}_v$ holds:

$$\mathbf{Q}_v = -\left(\frac{\partial \boldsymbol{\lambda}(\mathbf{q})}{\partial \mathbf{q}}\right)^\intercal \mathbf{D}(\mathbf{q}) \left(\frac{\partial \boldsymbol{\lambda}(\mathbf{q})}{\partial \mathbf{q}}\right) \dot{\mathbf{q}} \tag{9}$$

Noting the individual dependencies of the terms of $\mathcal{L}$ on $\mathbf{q}$, $\dot{\mathbf{q}}$, Eq. (7) takes the following form:

$$\frac{\mathrm{d}}{\mathrm{d}t}\frac{\partial K(\dot{\mathbf{q}})}{\partial \dot{\mathbf{q}}} + \frac{\partial U_m(\mathbf{q})}{\partial \mathbf{q}} - \frac{V^2}{2}\frac{\partial C(\mathbf{q})}{\partial \mathbf{q}} + \left(\frac{\partial \boldsymbol{\lambda}(\mathbf{q})}{\partial \mathbf{q}}\right)^{\intercal} \mathbf{D}(\mathbf{q}) \left(\frac{\partial \boldsymbol{\lambda}(\mathbf{q})}{\partial \mathbf{q}}\right) \dot{\mathbf{q}} = 0 \tag{10}$$

Algebraic manipulation of (4) shows that the first term of (10) is linear with $\ddot{\mathbf{q}}$ and independent of $\mathbf{q}$, $\dot{\mathbf{q}}$, i.e., the non-linearities described by the model only owe to the viscous and the static electro-elastic contributions. The input of the system is the voltage V, which appears in squared form into Eq. (10).To produce bi-directional oscillations of the DE membrane, the input voltage need to be the sum of a constant voltage bias, plus a time-varying term with variable sign. For the aim of sound reproduction (e.g., playing an audio file), choosing a time-dependent component of the voltage proportional to the desired output pressure will at least result in harmonic distortions due to the quadratic form of the voltage. For this reasons, different strategies have been proposed to suitably pre-process the voltage input as function of the desired acoustic output,[5,8,9] as further discussed in Sect. 4.

3.2 Radiated acoustic pressure model

The pressure field generated by the speaker is calculated from the local velocities of the DE diaphragm elements through a discretisation of the Rayleigh integral, which approximates the diaphragm surface as a distribution of acoustic monopoles.[9] In the following, we use a time-domain formulation for the Rayleigh integral, which accounts for the DE membrane curvature.[9,17]
We consider a cone-DEA mounted on an infinite baffle and a receptor point on the device axis at a distance h_r from the axis. With reference to Fig. 1 and considering the discretisation of the DEA surface, the radiated pressure can be expressed as:

$$p_a(h_r, t) = \rho_0 \sum_{k=1}^{n} \int_0^t G(d_k, d'_k, t, t') S_k \dot{\mathbf{v}}_k \cdot \mathbf{n}_k \mathrm{d}t' \tag{11}$$

where ρ_0 is the air density; S_k is the elemental area given by Eq. (6); $\mathbf{v}_k$ is the mean velocity and $\mathbf{n}_k$ the unit vector perpendicular to profile of the $k-$th element of the deformed membrane (Fig. 1), namely:

$$\mathbf{v}_k = -\frac{1}{2}\left[\dot{r}_{k-1} + \dot{r}_k,\ \dot{z}_{k-1} + \dot{z}_k\right]^{\intercal}, \quad \mathbf{n}_k = \frac{1}{\sqrt{(r_k - r_{k-1})^2 + (z_k - z_{k-1})^2}}\left[z_{k-1} - z_k,\ r_k - r_{k-1}\right]^{\intercal} \tag{12}$$

(for $k = 1$ and $k = n$ these relations take a slightly different form).
$G(d_k, t, t')$ is called the free-field Green function for a baffled surface, and it reads as follows:

$$G(d_k, d'_k, t, t') = \frac{\delta(t - t' - d_k/c_0)}{4\pi d_k} + \frac{\delta(t - t' - d'_k/c_0)}{4\pi d'_k} \tag{13}$$

where $\delta(\cdot)$ is the Dirac delta function, c_0 is the speed of sound in air, d_k is the distance of the receptor point from the mid-circumference of the $k-$th DE element, and d'_k is the distance of the receptor from the image points of the $k-$the element (i.e., the mirrored image of the element with respect to the baffle plane), namely:

$$d_k = \sqrt{\left(\frac{r_{k-1} + r_k}{2}\right)^2 + \left(h_r + \frac{z_{k-1} + z_k}{2}\right)^2}, \quad d'_k = \sqrt{\left(\frac{r_{k-1} + r_k}{2}\right)^2 + \left(h_r - \frac{z_{k-1} + z_k}{2}\right)^2} \tag{14}$$

The two distinct terms in the Green function account for the diaphragm curvature and the presence of the perfectly-reflecting baffle plane.

With the aim of putting pressure $p_a(h_r, t)$ into closer relation with the human perception of sound, the sound pressure level (SPL) is defined as follows:[20]

$$\mathrm{SPL} = 20\log_{10}\left(\frac{\tilde{p}_a}{p_{ref}}\right), \text{ with } \tilde{p}_a = \sqrt{\frac{1}{T}\int_0^T p_a^2 \mathrm{d}t}, \tag{15}$$

where $\tilde{p}_a$ denotes the root-mean-square pressure calculated over a time span T (e.g., one period, in the case of harmonic or periodic waves), and $p_{ref} = 20\ \mu$Pa is the reference human hearing threshold.

4. CASE STUDY

In this section, we present a case study on reference cone-DEA speaker, and analyse its performance using the model presented in Sect. 3. The features of the loudspeaker under investigation are similar to those of a prototype previously developed at the Intelligent Material System Laboratory, Saarland University.[21] The dimensions and material properties of the system are presented in Tab. 1. The DEA is assumed made of commercial silicone Elastosil 2030 films by Wacker Chemie AG.[22] A hyperelastic Yeoh model is used to describe the material elastic response, thus assuming the following expression for the strain-energy function as a function of the in-plane stretches, λ_1 and λ_2:[23]

$$\Psi(\lambda_1, \lambda_2) = C_{10}(I_1 - 3) + C_{20}(I_1 - 3)^2 + C_{30}(I_1 - 3)^3, \text{ with } I_1 = \lambda_1^2 + \lambda_2^2 + (\lambda_1\lambda_2)^{-2}, \tag{16}$$

where C_{10}, C_{20}, C_{30} are material constants.
In addition to the viscous damping of the DEA structure expressed through Eq. (9), we consider an additional damping contribution on coordinate z_n, accounted for by adding a term $B_{z_n}\dot{z}_n$ in the last component of $\mathbf{Q}_v$. This additional term accounts for damping effects associated with the pumping motion of the DEA, observed in low-frequency experiments.[15]

Kinematic parameters		**Material properties**	
r_i	16.5 mm		
r_o	36 mm	C_{10}	240 kPa
t_0	50 μm	C_{20}	-30 kPa
λ_p	1.2	C_{30}	20 kPa
n	5	η	600 Pa·s
Dynamic parameters		ε	$2.8 \cdot 8.85 \cdot 10^{-12}$ F/m
M_e	5 g	ρ_e	1.23 kg/m^3
k_e	50 N/m	B_{z_n}	0.65 kg/s
h_e	40 mm		

Table 1: Summary of the parameters used in the presented case study

We assume that thin polymer-based compliant electrodes are applied on the pre-stretched DE membrane. The stiffness of the electrodes is accounted for through the choice of the hyperelastic parameters,[23] and their mass is accounted for in the equivalent density ρ_e.

We consider a discretisation of the DE diaphragm made of $n = 5$ elements, whose edges are uniformly distributed along the pre-stretched membrane radius.
In all of the following analyses, we consider a receptor located on the DEA axis at a distance $h_r = 1$ m from the baffle plane.

In the following, we first validate the static multi-DoF model against a finite element method (FEM) model of the system. We then investigate the mode shapes of the linearised DEA response, and weight their effect on the loudspeaker frequency response. Finally, we investigate the effects of the DEA nonlinear response and different control strategies in terms of the loudspeaker harmonic distortion.

4.1 Comparison with finite element solution

With the aim of validating the multi-DoF model presented in Sect. 3.1, we compare the static response of the membrane with that obtained through a FEM continuum formulation. A static axial-symmetrical FE model has been implemented in Comsol Multiphysics 5.6 using membrane structural elements and the in-built nonlinear structural mechanics module. The electro-elastic coupling has been implemented in a simplified manner, by adding a term in the equation of the in-built strain-energy function so as to include the contribution of the electrostatic co-energy.[24] This latter electrostatic term is a function of the user-defined voltage difference applied on the membrane element faces. In the FEM model, the geometry is discretised using 450 nodes along the radius.

Fig. 2a shows a comparison of the equilibrium profile of the cone DEA, under the action of the biasing spring, in the discharged state and in the presence of a constant applied voltage $V = 2.5$ kV (roughly, 80 kV/mm

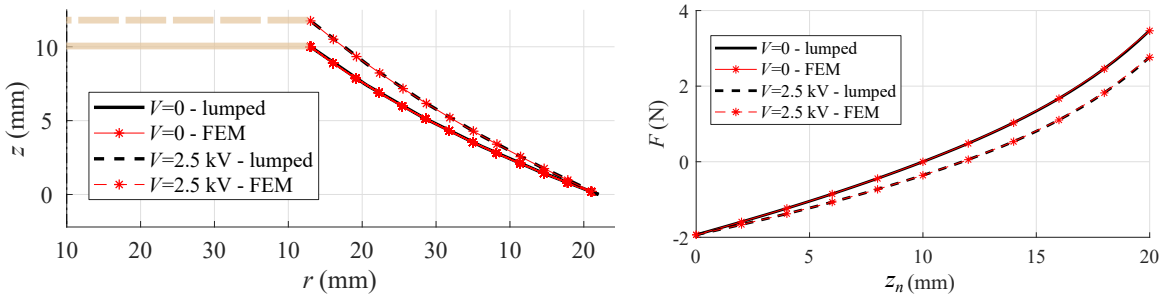

(a) (b)

Figure 2: Validation of the proposed cone DEA model model against a coupled-electro mechanical FEM model. (a) Comparison of the DEA equilibrium profiles at $V = 0$ and $V = 2.5$ kV. (b) Force-displacement characteristic of the DEA at $V = 0$ and $V = 2.5$ kV.

maximum electric field). Despite the rather coarse discretisation of the domain, our model is able to capture the DEA deformed shape with great accuracy. Compared with single-DoF models, which assume that the deformed membrane has the shape of a truncated cone,[14,15] the model effectively describes the necking effects on the membrane profiles.

Assuming that the DEA system (i.e., the combination of the DEA membrane and the biasing spring) is subject to an external axial force F applied on the rigid disc, Fig. 2b relates F to the central disc position, both in the inactive state and at 2.5 kV. The presence of a constant force F is accounted for in the lumped-parameter model through an additional term in the last component of Eq. (10). In the plots, the $F = 0$ is associated with the equilibrium value of z_n. The plot confirms the ability of the proposed formulation to accurately capture the device static response.

4.2 Mode shapes and frequency response

As a first step towards the analysis of a DE loudspeaker, it is convenient to linearise the DEA dynamics (Eq. (10)) and the output pressure equation (11). Doing so makes it possible to visualise the different vibration regimes of the system (namely, the mode shapes), and weight their contribution on the output pressure throughout the frequency range.

We linearise the DEA dynamics by assuming that the input voltage is the sum of a constant bias voltage V_0 plus a small-amplitude time-varying component $\delta V(t)$:

$$V(t) = V_0 + \delta V(t) \implies V^2(t) \simeq V_0^2 + 2V_0\delta V(t). \tag{17}$$

Indicating with $\mathbf{q}_0$ the equilibrium position of the system under the effect of constant voltage V_0, the linearised equations of motion read as:

$$\begin{gathered}\mathbf{M}\ddot{\mathbf{q}} + \mathbf{B}\dot{\mathbf{q}} + \mathbf{K}\mathbf{q} = \mathbf{d}(t), \text{ with } \mathbf{M} = \frac{\partial^2 K(\dot{\mathbf{q}})}{\partial \dot{\mathbf{q}}^2}, \\ \mathbf{B} = \left(\frac{\partial \boldsymbol{\lambda}(\mathbf{q})}{\partial \mathbf{q}}\right)^{\intercal}_{\mathbf{q}=\mathbf{q}_0} \mathbf{D}(\mathbf{q}_0) \left(\frac{\partial \boldsymbol{\lambda}(\mathbf{q})}{\partial \mathbf{q}}\right)_{\mathbf{q}=\mathbf{q}_0}, \ \mathbf{K} = \left(\frac{\partial^2 U_m(\mathbf{q})}{\partial \mathbf{q}^2}\right)_{\mathbf{q}=\mathbf{q}_0} - \frac{V_0^2}{2}\left(\frac{\partial^2 C(\mathbf{q})}{\partial \mathbf{q}^2}\right)_{\mathbf{q}=\mathbf{q}_0}, \\ \mathbf{d}(t) = 2V_0\delta V(t)\left(\frac{\partial C(\mathbf{q})}{\partial \mathbf{q}}\right)_{\mathbf{q}=\mathbf{q}_0}\end{gathered} \tag{18}$$

The eigenfrequencies and eigenmodes of the undamped system can be thus calculated as:

$$\mathbf{K}\ \delta\mathbf{q}_{0i} = \omega_{0i}^2 \mathbf{M}\ \delta\mathbf{q}_{0i},\ i = 1, \ldots, 2n-1, \tag{19}$$

where ω_{0i} are the natural angualar frequencies of the system, and $\delta\mathbf{q}_{0i}$ the corresponding mode shapes (that have the meaning of displacements from the equilibrium configuration $\mathbf{q}_0$).

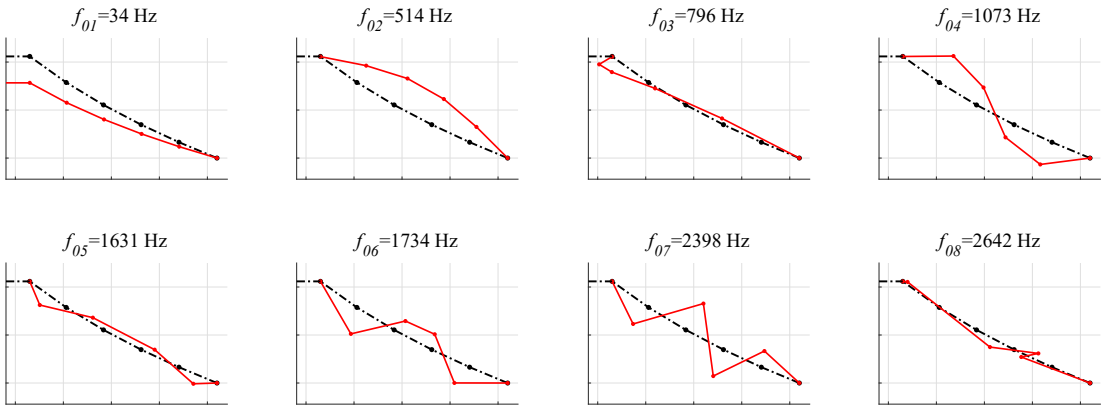

Figure 3: Axial-symmetrical mode shapes and corresponding natural frequencies of the DEA system. The black dash-dot line represents the equilibrium configuration, whereas the red solid line represents the deformation associated with the mode.

Equation (19) shows that discretising the DE membrane into n elements allows for the calculation of the first $2n-1$ modes. In practice, this sets an upper bound to the frequency range that can be consistently analysed with such a discretisation.

Here, we consider frequencies up to 3000 Hz, and we thus consider the mode shapes with natural frequency $f_{0i} = \omega_{0i}/(2\pi) < 3000$ Hz, which are represented in Fig. 3.
The first mode is the so-called pumping-mode, rendering the pistonic motion of the DEA, i.e., a displacement of the central disc. In all of the other modes, the central disc does not move, and the system motion is governed by the structural dynamics of the DE membrane. The frequency gap between the pumping mode and the second mode is larger than the gap between consecutive structural modes. This frequency and the shape of the higher-order modes (with $z_n = 0$) owe to the large mass of the central disc, which is orders of magnitude larger than the mass of the lightweight membrane elements. This confirms that the cone DEA motion can be considered pistonic (and described through a single DoF) over a wide low-frequency band.[14,15]
The higher-order structural modes can be compared with known solutions for the structural modes of a tensioned annular membrane with fixed edges.[25,26] In particular, modes $i = 2, 4, 6$ and 7 compare with the first 4 axial-symmetrical modes of an annular membrane vibrating out-of-plane, hence, they are characterised by transverse displacement of the membrane nodes. In contrast, modes $i = 3, 5$ and 8 cannot be compared/associated with any of the flat annular membrane modes. In effect, these modes are triggered by radial displacements of the membrane elements (as opposed to axial displacements), and are specific of the out-of-plane mechanical biasing applied on the membrane.

In order to evaluate the contribution of the different modes on the acoustic response, we calculate the SPL radiated of the DE loudspeaker in the case of small-amplitude harmonic linear vibrations. To this end, we assume that a sinusoidal excitation $\delta V(t)$ with amplitude V_a and given frequency is applied on the DEA, and we solve linear dynamics (18). We then use this harmonic solution to calculate the sound pressure p_a at the receptor point through (11) and, hence, the SPL (Eq. (15)). Notice that, using the coordinates of the equilibrium point $\mathbf{q}_0$ to evaluate $\mathbf{n}_k$ (Eq. (12)) and the Green function (13), relationship (11) between p_a and the DE nodes velocity is linear, and can be easily reformulated in the frequency-domain.[9] Figure. 4a shows the SPL as a function of the input frequency, assuming $V_0 = 1.5$ kV and $V_a = 200$ V.

The high modal density within the considered range causes the loudspeaker's frequency response to considerably deviate from the ideal flat profile. The frequency response of the loudspeaker is characterised by resonance-antiresonance peak-valley sequences typical of multi-DoF oscillators. The peaks dwell in correspondence of some of the natural frequencies shown in Fig. 3. Interestingly, peaks are only associated with the modes induced by transverse deformations of the membrane, whereas modes i =3, 5 and 8, originated by the radial

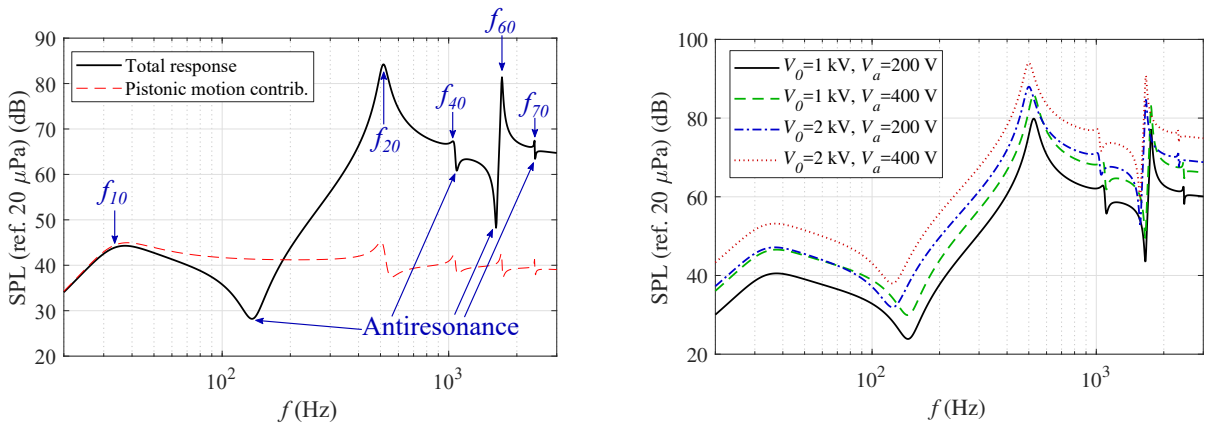

(a) (b)

Figure 4: (a) SPL at 1 m distance, when the reference DE speaker is driven with a sinusoidal voltage with bias $V_0 = 1.5$ kV and amplitude $V_a = 200$ V. The dashed line represents the contribution ascribable to the pistonic motion of the speaker. (b) Influence of the bias value and amplitude of the input voltage on the SPL.

degrees of freedom of the membrane, do not induce any peak in the SPL curve and are thus of little interest from an acoustic perspective. The highest SPL is generated by modes 2 and 6. The SPL in the low-frequency range is significantly lower than at higher frequencies.
In order to isolate the contribution of the pumping mode, we projected the velocity distribution obtained from Eq. (18) along eigenmode $\delta\mathbf{q}_{01}$, and fitted the resulting velocity profile into (11). The fraction of the SPL associated with the pumping mode is represented by the dashed line in Fig. 4a. Interestingly and in contrast with traditional electrodynamic speakers,[20] only a minor fraction of the SPL can be here ascribed to the speaker's pumping mode, whereas a major contribution is provided by the higher order modes over most of the frequency range.

Figure 4b shows the influence of the voltage bias and amplitude on the SPL. Increasing the amplitude of the excitation increases the deformation amplitudes and, hence, the SPL (under the assumption of linear dynamics, the amplitude of p_a is proportional to V_a). Increasing the bias voltage V_0 generates a reduction in the stress acting on the membrane (due to Maxwell stress), leading to an increase in the SPL and a decrease in the natural frequencies of the different modes.

4.3 The effects of the non-linearities on the loudspeaker harmonic distortion

This section investigates the influence of the nonlinear DEA dynamics on the acoustic response. The effect of the nonlinearities is evaluated through the total harmonic distortion (THD) of the output pressure with respect to a target harmonic output. In the presence of a periodic excitation with frequency f, the steady-state DEA response ca be represented via a Fourier series, namely: $p_a(t) = \sum_{k=1}^{+\infty} P_k \sin(2\pi k f t)$. The THD is defined accordingly as:

$$\mathrm{THD} = \frac{\sqrt{\sum_{k=1}^{+\infty} P_k^2}}{P_1}. \tag{20}$$

Aiming to produce monochromatic pressure outputs, we compare two alternative choices for the driving voltage, namely a sinusoidal excitation, and a square-rooted sinusoidal excitation, which compensates the nonlinear (quadratic) dependency of (10) on the voltage:

- Sinusoidal voltage:
$$V(t) = V_0 + V_a \sin(2\pi f t); \tag{21}$$
- Square-rooted sinusoidal voltage:
$$V(t) = \sqrt{V_0^2 + V_a^2 + 2V_0 V_a \sin(2\pi f t)}. \tag{22}$$

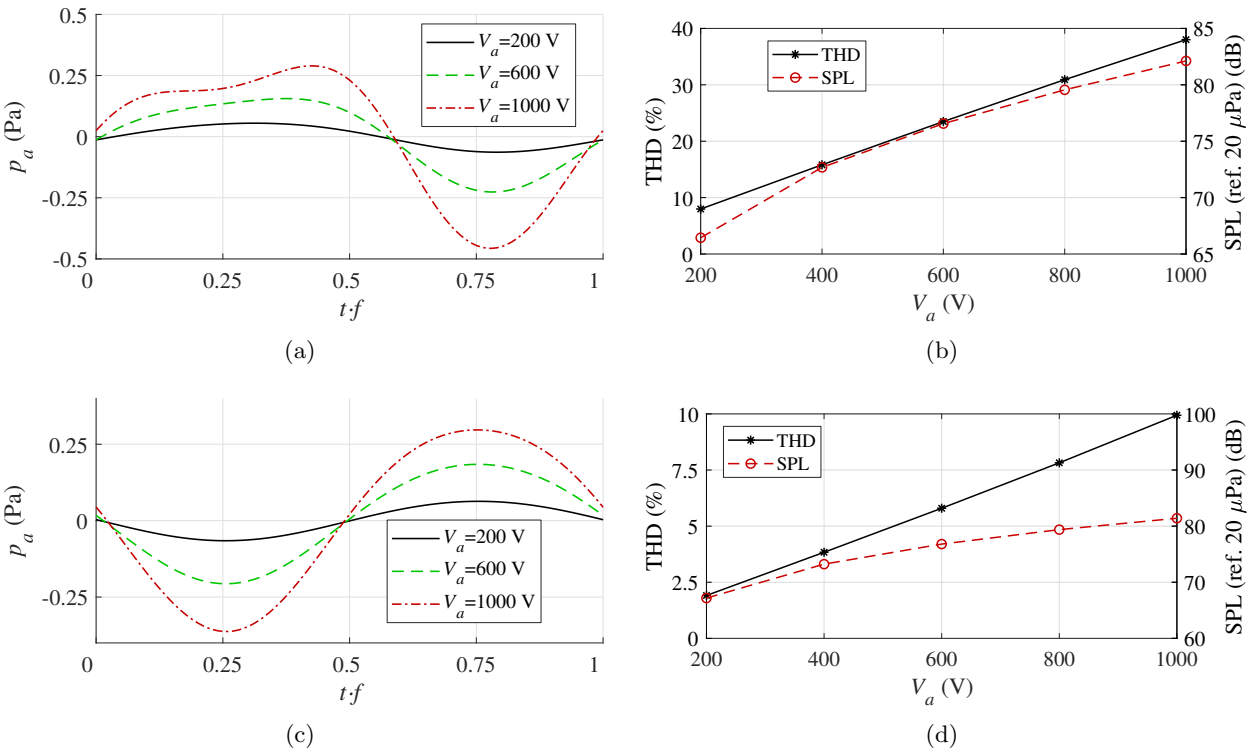

Figure 5: Effect of the driving voltage amplitude on the distortion for a sinusoidal excitation (waveform (21)) with bias $V_0 = 1.5$ kV. (a, c) Sound pressure waveform, and (b,d) SPL and THD vs. V_a at 400 and 2000 Hz respectively.

With both waveforms, the maximum voltage on the DEA equals $V_0 + V_a$. Fitting waveform (21) into (10) results in a multi-chromatic excitation (i.e., $V^2(t) = V_0^2 + 0.5V_a^2 + 2V_0V_a\sin(2\pi ft) - 0.5V_a^2\cos(4\pi ft)$), whereas (22) provides the system with a monochromatic input.
We simulated the nonlinear response of the cone DEA loudspeaker by scripting the model presented in Sect. 3 in Matlab & Simulink. The first 10 harmonics of the Fourier-series decomposition of the steady-state outputs were calculated for the evaluation of the THD.

With reference to a sinusoidal input voltage (Eq. (21)), Fig. 5 compares the SPL and THD obtained with different amplitudes, at two different frequencies ($f = 400$ and 2000 Hz). As expected, the THD is larger in the low frequency range, where higher order harmonics are radiated more efficiently than the fundamental.[27] The plots show that the generated pressure significantly deviates from the sinusoidal profile at low frequency, while a lower level of distortion occurs at higher frequency. Increasing the driving voltage amplitude generates an increase both in the SPL and the THD (though the latter exhibits a steeper increase). At low frequencies, the THD ranges from 10 to 40%, while at 2 kHz it is in the range 2-10% at 2 k Hz (just-detectable harmonic distortions for the human hear are in the order of 1%[28]).

To measure to what extent the observed distortions owe to the choice of a sinusoidal voltage excitation, in Fig. 6 we compare the pressure output profiles and the THD obtained with the waveforms in (21) and (22). Employing waveform (22) leads to a clear reduction in the THD. With this driving strategy, the total distortion is roughly halved at 400 Hz and decreased by a factor 4 at 2000 Hz (see Figs. 6b and 6d). The remaining distortion owes to the nonlinearities in the DEA dynamics. The pressure amplitude is similar at the two frequencies under investigation (Fig. 6a, Fig. 6c), indicating that the deformation amplitudes are larger at the lower frequency. As a result, the low frequency response is more affected by nonlinearity, even in the presence of a square-rooted sine input.

A comparison of the sinusoidal and square-rooted sinusoidal waveforms over the reference frequency range

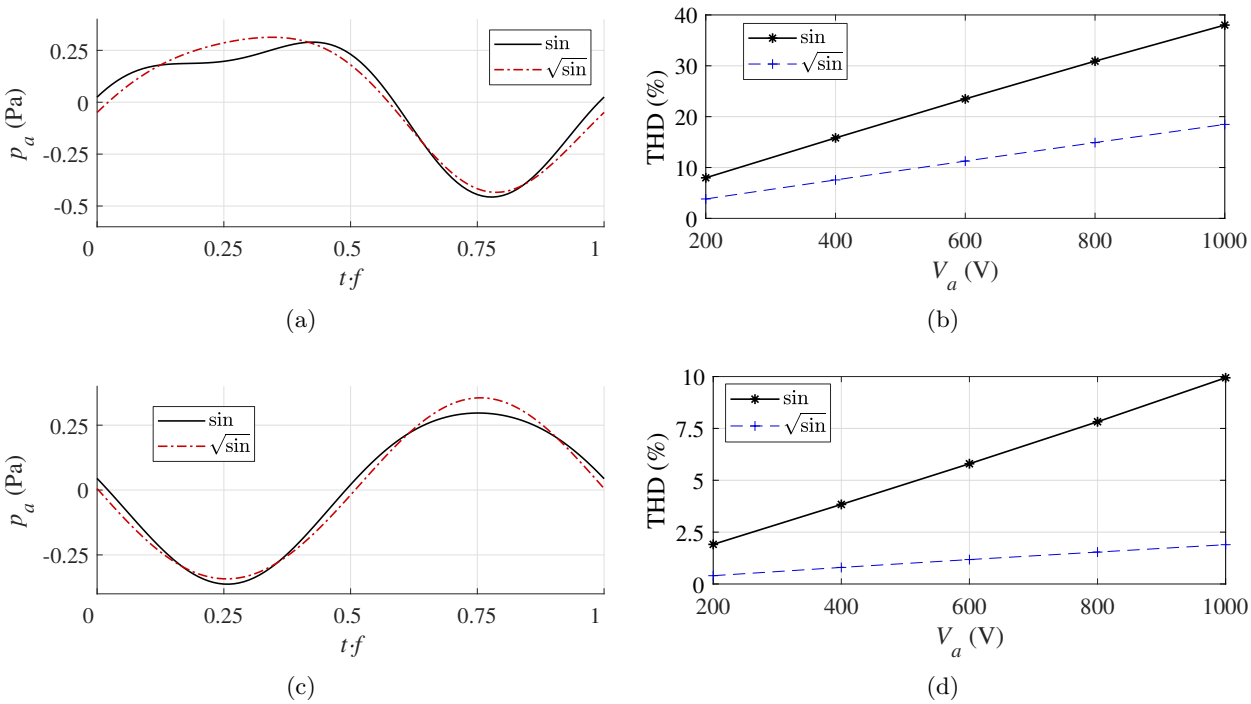

Figure 6: Comparison of the sinusoidal and square-rooted sinusoidal driving waveforms in terms of the loudspeaker distortion. (a, c) Sound pressure wave forms at $V_a = 1$ kV, and (b, d) THD as a function of V_a at 400 and 2000 Hz respectively. In all plots, $V_0 = 1.5$ kV.

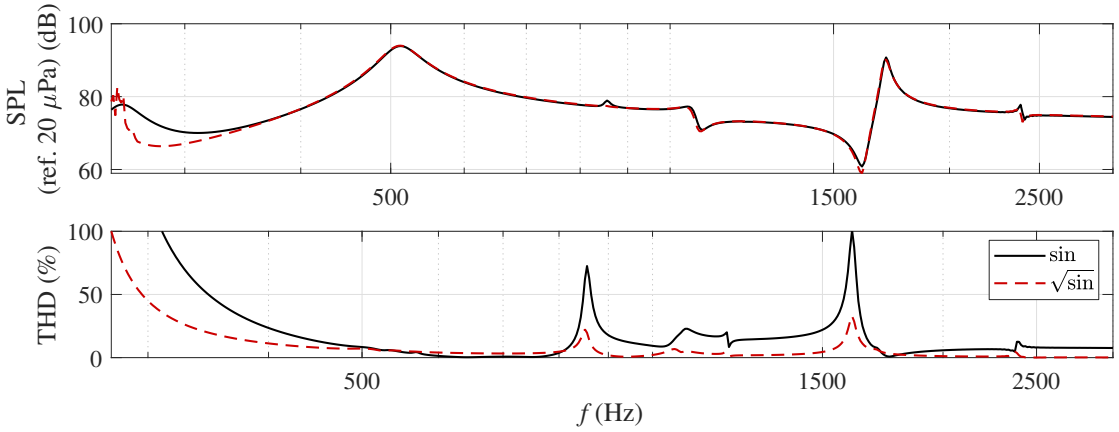

Figure 7: SPL and THD as a function of the excitation frequency, for a speaker subject to a driving voltage with $V_0 = 1.5$ kV and $V_a = 600$ V, respectively with sinusoidal (Eq. 21) and square-rroted sinusoidal (Eq. 22) waveforms.

is shown in Fig. 7. The plot summarises shows the SPL and THD obtained at values of f, with bias voltage $V_0 = 1.5$ kV and amplitude $V_a = 600$ V (Eq. (21)-(22)). Waveforms (21) or (22) provide nearly identical values of the SPL over most of the frequency range, whereas waveform (22) leads to a reduction in the THD. The THD has an average decreasing trend with the frequency, though it experiments local maxima in correspondence of the diaphragm natural frequencies (see also Fig. 4a), where the membrane displacements (and, hence, the nonlinearities) are maximum.

4.4 Discussion

The presented simulation results show that the structural natural frequencies and mode shapes (Fig. 3) of the DE diaphragm strongly influence the acoustic frequency response of the DE loudspeaker. Traditional loudspeakers with stiff diaphragm typically work in a frequency range comprised between the pumping mode natural frequency and the frequency of the second mode (called a breakup mode).[20] In the cone DEA speaker, the pumping mode plays a minor role on the sound generation, since a large number of structural higher order modes fall within the acoustic range (Fig. 4a). The natural frequencies of pre-stressed membranes are roughly proportional to the square root of the stress divided the density, and inversely proportional to the radial dimensions.[25] To move the structural resonances of a DE membrane at the upper bound of the frequency ranges of interest, unusually stiff DE materials or very small dimensions for the active diaphragms should be selected. In the literature, this has been implicitly attempted through the implementation of arrays of small DE speaker units.[5,8] Nonetheless, designing a DE speaker whose operating range is completely free from higher-order modes seems a very complicated task. Although improvements in the uniformity of the frequency response can be potentially achieved through control, it is clear that DEs are not ideal candidates for hi-fi audio application, whereas they clearly represent a promising option for lightweight highly-integrated soft acoustic actuators.

The analytical approach pursued here has some limitations, that will be addressed in the future. Using a discretisation of the DE membrane like that proposed here (Fig. 1) limits the frequency range that can be analysed. A modal decomposition could be used instead, hence representing the DEA deformation as a superposition of the contributions of the modes.
The prominence of the peaks in the frequency response strongly depend on the structural damping, which is here modelled in a rather simplistic manner (Eq. (8)). Available estimates of the viscoelastic properties of DEs come from low frequency experiments on devices operating in the pumping regime.[15,18] More accurate characterisations and improved constitutive models needs to be developed in order to capture DEs' response at high frequencies.
The proposed model does not account for the effect of the compliant electrodes resistivity, and the acoustic loading of the DE membranes, which have been recently shown to play a relevant role in DEA acoustic applications.[13,29] The acoustic impedance might also play an important role, providing the loudspeaker with additional fluid-borne inertia and hence lowering the natural frequencies of the structural modes. Here, e.g., the acoustic added mass associated with mode 02 (Fig. 3) can be roughly approximated as the added mass of a pumping ring source.[30] Such an added mass can be as high as 50%-60% of the DE membrane mass, virtually leading to reductions of at least 20% in the natural frequency of mode 02. Moving from a partially-coupled approach, like that presented here, to fully-coupled models[13] is therefore a necessary step, in order to consistently account for the significant contribution of the acoustic impedance.
Screen-printed silicone electrodes with thickness in the range 1-10 μm have a sheet resistance on the order of 100 k$\Omega/\square$.[31] In a DEA similar to that studied here (Tab. 1), this results in charging times on the order of ~ 0.1 ms, and is thus not expected to significantly affect the frequency range considered here, although it could be relevant at higher frequencies.
Finally, extensive experimental validation in support of the proposed model needs to be pursued, combining acoustic measurements, and structural vibration measurements.[16]

5. CONCLUSIONS

This paper presents a theoretical analysis of a cone-shaped dielectric elastomer (DE) loudspeaker. In contrast with traditional electrodynamic loudspeakers, in DE-based acoustic devices the vibrating diaphragm and the actuator are integrated into a single stretchable rubber-like membrane, leading to lightweight low-cost solutions. Here, we propose an axial-symmetric multi-degree-of-freedom model of the cone DE actuator (DEA), and employ it to predict the generated pressure field. As opposed to previous works on the cone DEA, here we model the actuator as a multi-degree-of-freedom system, hence accounting for the effect of nonlinear structural vibrations. Via numerical simulations, we highlight the effect of the system's eigenmodes on the acoustic frequency response. In particular, we demonstrate that the speaker pumping mode only accounts for a fraction of the total power radiated in the relevant acoustic range, whereas a major role is played by higher order modes. Then, we investigate the effect of the loudspeaker dynamics nonlinearities on the total harmonic distortion, comparing the

performance of different driving strategies, namely, a harmonic sinusoidal voltage input, and a square-rooted input aimed at compensating the quadratic voltage-deformation nonlinearity inherent to DEAs.
Future developments will be focused on the analysis of three-dimensional mode-shapes and their contribution on the acoustic response, the evaluation of the acoustic loads on the DE membrane dynamics, and the validation of the model through experiments.

ACKNOWLEDGMENTS

This project has received funding from the European Union's Horizon 2020 research and innovation programme under the Marie Skłodowska-Curie grant agreement No 893674 (DEtune).

REFERENCES

[1] Pelrine, R., Kornbluh, R., Pei, Q., and Joseph, J., "High-speed electrically actuated elastomers with strain greater than 100%," *Science* **287**(5454), 836–839 (2000).

[2] Gu, G.-Y., Zhu, J., Zhu, L.-M., and Zhu, X., "A survey on dielectric elastomer actuators for soft robots," *Bioinspiration & biomimetics* **12**(1), 011003 (2017).

[3] Cao, C., Gao, X., and Conn, A. T., "A magnetically coupled dielectric elastomer pump for soft robotics," *Advanced Materials Technologies* **4**(8), 1900128 (2019).

[4] Heydt, R., Kornbluh, R., Pelrine, R., and Mason, V., "Design and performance of an electrostrictive-polymer-film acoustic actuator," *Journal of Sound and Vibration* **215**(2), 297–311 (1998).

[5] Heydt, R., Pelrine, R., Joseph, J., Eckerle, J., and Kornbluh, R., "Acoustical performance of an electrostrictive polymer film loudspeaker," *The Journal of the Acoustical Society of America* **107**(2), 833–839 (2000).

[6] Hochradel, K., Rupitsch, S., Sutor, A., Lerch, R., Vu, D., and Steinmann, P., "Dynamic performance of dielectric elastomers utilized as acoustic actuators," *Applied Physics A* **107**(3), 531–538 (2012).

[7] Hosoya, N., Baba, S., and Maeda, S., "Hemispherical breathing mode speaker using a dielectric elastomer actuator," *The Journal of the Acoustical Society of America* **138**(4), EL424–EL428 (2015).

[8] Klug, F., Endl, C., Solano-Arana, S., and Schlaak, H. F., "Design, fabrication, and customized driving of dielectric loudspeaker arrays," in [*Electroactive Polymer Actuators and Devices (EAPAD) XXI*], **10966**, 109662I, International Society for Optics and Photonics (2019).

[9] Garnell, E., Rouby, C., and Doaré, O., "Dynamics and sound radiation of a dielectric elastomer membrane," *Journal of Sound and Vibration* **459**, 114836 (2019).

[10] Rustighi, E., Kaal, W., Herold, S., and Kubbara, A., "Experimental characterisation of a flat dielectric elastomer loudspeaker," in [*Actuators*], **7**(2), 28, Multidisciplinary Digital Publishing Institute (2018).

[11] Gareis, M. and Maas, J., "Acoustical behaviour of buckling dielectric elastomer actuators," in [*Smart Materials, Adaptive Structures and Intelligent Systems*], **59131**, V001T02A014, American Society of Mechanical Engineers (2019).

[12] Sugimoto, T., Ando, A., Ono, K., Morita, Y., Hosoda, K., Ishii, D., and Nakamura, K., "A lightweight push-pull acoustic transducer composed of a pair of dielectric elastomer films," *The Journal of the Acoustical Society of America* **134**(5), EL432–EL437 (2013).

[13] Garnell, E., Doaré, O., and Rouby, C., "Coupled vibro-acoustic modeling of a dielectric elastomer loudspeaker," *The Journal of the Acoustical Society of America* **147**(3), 1812–1821 (2020).

[14] Berselli, G., Vertechy, R., Vassura, G., and Parenti-Castelli, V., "Optimal synthesis of conically shaped dielectric elastomer linear actuators: design methodology and experimental validation," *IEEE/ASME Transactions on Mechatronics* **16**(1), 67–79 (2011).

[15] Rizzello, G., Hodgins, M., Naso, D., York, A., and Seelecke, S., "Modeling of the effects of the electrical dynamics on the electromechanical response of a DEAP circular actuator with a mass–spring load," *Smart Materials and Structures* **24**(9), 094003 (2015).

[16] Nalbach, S., Rizzello, G., and Seelecke, S., "Experimental analysis of continuous vibrations in dielectric elastomer membrane actuators via three-dimensional laser vibrometry," *Journal of Vibration and Acoustics* **141**(5) (2019).

[17] Quaegebeur, N., Chaigne, A., and Lemarquand, G., "Transient modal radiation of axisymmetric sources: Application to loudspeakers," *Applied Acoustics* **71**(4), 335–350 (2010).

[18] Rizzello, G., Serafino, P., Naso, D., and Seelecke, S., "Towards sensorless soft robotics: Self-sensing stiffness control of dielectric elastomer actuators," *IEEE Transactions on Robotics* **36**(1), 174–188 (2019).

[19] Zhang, J., Ru, J., Chen, H., Li, D., and Lu, J., "Viscoelastic creep and relaxation of dielectric elastomers characterized by a Kelvin-Voigt-Maxwell model," *Applied Physics Letters* **110**(4), 044104 (2017).

[20] Kleiner, M., [*Acoustics and audio technology*], J. Ross Publishing, Fort Lauderdale, FL (2011).

[21] "MeloDEA: A Dielectric Elastomer Actuator based Loudspeaker." http://https://www.youtube.com/watch?v=CJy2LCIpuZs&ab_channel=intelligentMaterialSystemsLab.

[22] "Elastosil films catalogue, Wacker." https://https://www.wacker.com/h/en-us/silicone-rubber/silicone-films/elastosil-film-2030/p/000038005.

[23] Rizzello, G., Loew, P., Agostini, L., Fontana, M., and Seelecke, S., "A lumped parameter model for strip-shaped dielectric elastomer membrane transducers with arbitrary aspect ratio," *Smart Materials and Structures* **29**(11), 115030 (2020).

[24] Vertechy, R., Frisoli, A., Bergamasco, M., Carpi, F., Frediani, G., and De Rossi, D., "Modeling and experimental validation of buckling dielectric elastomer actuators," *Smart Materials and Structures* **21**(9), 094005 (2012).

[25] Sharp, G. R., "Finite transform solution of the symmetrically vibrating annular membrane," *Journal of Sound and Vibration* **5**(1), 1–8 (1967).

[26] Jabareen, M. and Eisenberger, M., "Free vibrations of non-homogeneous circular and annular membranes," *Journal of Sound and Vibration* **240**(3), 409–429 (2001).

[27] Klippel, W., "Loudspeaker nonlinearities–causes, parameters, symptoms," in [*Audio Engineering Society Convention 119*], Audio Engineering Society (2005).

[28] Self, D., [*Audio power amplifier design handbook*], Elsevier (2002).

[29] Garnell, E., Rouby, C., and Doaré, O., "Resistivity-induced coupling between voltage distribution and vibrations in dielectric elastomers," *Smart Materials and Structures* (2020).

[30] Thompson Jr, W., "The computation of self-and mutual-radiation impedances for annular and elliptical pistons using Bouwkamp's integral," *Journal of Sound and Vibration* **17**(2), 221–233 (1971).

[31] Fasolt, B., Hodgins, M., Rizzello, G., and Seelecke, S., "Effect of screen printing parameters on sensor and actuator performance of dielectric elastomer (de) membranes," *Sensors and Actuators A: Physical* **265**, 10–19 (2017).

View publication stats